Engineering Structures 57 (2013) 23–36

Contents lists available at ScienceDirect

Engineering Structures

journal homepage: www.elsevier.com/locate/engstruct

Strengthening of RC one-way slabs including cut-out using different techniques ☆

H.M. Afefy *, Tarek Mohamed Fawzy

Structural Engineering Dept., Faculty of Engineering, Tanta University, Tanta, Egypt

ARTICLE INFO

Article history:
Received 15 July 2013
Revised 6 September 2013
Accepted 9 September 2013
Available online 8 October 2013

Keywords:
Cut-outs
Carbon Fiber Reinforced Polymer (CFRP) anchors
CFRP sheet
Engineered Cementitious Composites (ECC)
Near Surface Mounted (NSM)-steel bar
RC slabs
Strengthening

ABSTRACT

Often, it is essential to introduce a cut-out in an existing reinforced concrete slab for facility requirements. That cut-out poses a break in the continuity of the slab loading trajectories. Hence, a great attention has to be paid to the adopted strengthening approach in order to restore the flexural resistance of the slab included cut-out. To investigate the structural flexural performance of strengthened one-way reinforced concrete slab included cut-out, six slabs including cut-out adjacent to the central patch load in addition to one slab without cut-out as a reference slab were tested up to failure under incremental monotonic loading. The six slabs including cut-outs contained one control un-strengthened slab along with five strengthened slab. These slabs were strengthened using either Near Surface Mounted (NSM) steel bars or Externally Bonded Carbon Fiber Reinforced Polymer (EB-CFRP) at the tension side, while four out of them were strengthened by either NSM-steel bars (one slab) or an overlay of Engineered Cementitious Composites (ECC) material (three slabs) at the compression side. It can be concluded that end anchors for the EB-CFRP sheets along with the surface preparation before installing the ECC overlay are very important parameters in order to guarantee the optimum utilization for both the EB-CFRP sheets and the ECC overlay material. In addition, the test results showed that the hybrid strengthening technique incorporated NSM-steel bars in tension side along with ECC overlay in compression side showed its superiority among all proposed strengthening schemes. It is not only allowed the slab included cut-out to restore its flexural resistance, but also it enabled the slab to outperform its structural performance compared to that of the slab without cut-out.

© 2013 Elsevier Ltd. All rights reserved.

1. Introduction

Introducing cut-outs in an existing reinforced concrete slab is necessary in some circumstances as the installation of escalators, elevators or utilities such as air conditioning, heating or wiring ducts. These cut-outs have the advantages of improved air circulation, aesthetics, and improved lighting. However, these cut-outs pose a break in the continuity of the slab causing weak points in the whole structure. They thus require special attention in remodeling of the slab in order to capture the actual behavior of the new slab including cut-out [1–4].

Broad applications of the fiber-reinforced polymer (FRP) materials as new construction strengthening materials have been recently accomplished. FRP materials are lightweight, high strength, and non-corrosive materials. By virtue of these advantages, there are wide ranges of recent, current, and potential applications of these materials that cover both new and existing structures. Among different types of FRP materials, a Carbon Fiber Reinforced Polymer (CFRP) is used extensively in the structural engineering field. The Externally Bonded Reinforcement (EBR) technique has been more generally applied due to its simple installation procedure. Design guidelines and specifications have also been established well for this system [5]. In particular, their practical implementations for strengthening by epoxy bonding are several [6–10].

When compared to the Externally Bonded Reinforcement (EBR) technique, the Near Surface Mounted (NSM) technique assures a higher anchoring capacity to the CFRP reinforcing material. In consequence, a high tensile stress can be mobilized in the CFRP, as long as the member load carrying capacity is not limited by a premature failure mode [11–13]. The Near-Surface Mounted (NSM-CFRP) strengthening technique has been used in the recent years, with remarkable efficiency, in order to increase the flexural strength [14,15]. The use of FRP rods for this application is very new and the Near Surface Mounted (NSM) steel rods have been in Europe for strengthening of RC structures dated back to 1948 [16].

☆ The experimental work had been conducted at Tanta University's Concrete and Heavy Structures Laboratory.

* Corresponding author. Address: 34 Ahmed Farouk Ali Ezzat, Smouha, Alexandria, Egypt. Tel.: +20 3 4298 793, mobile: +20 106 177 3174.

E-mail addresses: hamdyafefy@hotmail.com (H.M. Afefy), telakrat1@yahoo.com (T.M. Fawzy).

0141-0296/$ - see front matter © 2013 Elsevier Ltd. All rights reserved.
http://dx.doi.org/10.1016/j.engstruct.2013.09.013

For RC slabs of low or medium concrete strength, the increment of the flexural resistance that NSM can provide might be limited by the maximum allowable compressive strain in the extreme compressed concrete fiber. This drawback can be overcome by adding a concrete layer in the compression zone of the existing slab [17,18]. In order to achieve the desired full composite action, the new concrete overlay and the existing concrete slab should behave monolithically. A sound bond between the new layer and the existing concrete slab can be guaranteed if a proper epoxy compound is used [19,20].

Another way of strengthening of RC slabs is adding a new concrete layer. The additional concrete overlay increases the lever arm of the moment resisting of the concrete section. Casting an overlay and thus adjoining a fresh material onto an older structure can result in durability problems such as cracking and de-lamination along the transition zone between the two materials. These occurrences are mostly dependent on differential movements, i.e. volume changes, between the base concrete and the overlay caused by shrinkage, temperature variations or both, poor workmanship or external loads [21,22].

Engineered Cementitious Composites (ECC) is an exceptional representative of the new generation of high performance fiber reinforced cementitious composites, featuring high ductility and durability characteristics [23–26]. ECC's high tensile ductility, deformation compatibility with existing concrete, and self-controlled micro-crack width lead to its superior durability under various mechanical and environmental loading conditions such as fatigue, freezing and thawing, chloride exposure, and drying shrinkage [27–29]. Engineered Cementitious Composites (ECC) is a mortar-based composite that is reinforced with short random fibers, such as polyethylene (PE) or polyvinyl alcohol (PVA). The use of PVA fibers has better tensile crack bridging properties while the use of PE fibers shows a better compressive behavior [30]. ECC is a micromechanically designed material that uses a micromechanical model to tailor-make the required properties. By using this micromechanical tool, the fiber amount used in the ECC is typically 2% by volume. Thus, ECC is designed to resist large tensile and shear forces but at the same time has compatible properties, such as compressive strength and thermal expansion, to ordinary concrete based on Portland cement [31].

Experimental investigations on the structural performance of one-way spanning CFRP-strengthened slabs with cut-outs have been reported by Alkhrdaji et al. [32], Vasquez and Karbhari [33], Casadei et al. [34], Tan and Zhao [35] and Smith and Kim [1]. They concluded that FRP-strengthened slabs achieved a higher load-carrying capacity than their un-strengthened control counterparts. In addition, all strengthened slabs failed by de-bonding initiating at intermediate cracks (IC de-bonding) and in the case of the slabs with cut-outs, the critical cracks were diagonal and originated from the corners of the cut-out. Boon et al. [2] showed that the effect of additional rectangular bars along with diagonal bars surrounding the opening failed to restore the bending capacity of un-cut slab. Seliem et al. [36] showed that the slab included cut-outs strengthened with NSM-CFRP strips had a higher load-carrying capacity in comparison to the slab strengthened with EB-CFRP laminates while using significantly less area of FRP. This behavior is attributed to the improved resistance of the NSM technique to IC de-bonding. Kim and Smith [4] showed that the FRP anchors were found to increase the strength of RC slabs with large penetrations and delay complete loss of the strengthening plates due to de-bonding.

For the made cut-out in reinforced concrete slabs, the common practice is to replace the cut reinforcement around the opening without compensation of the concrete part [3]. However, the cut-out involves both concrete and reinforcing steel. The reinforced concrete section always is designed in order to withstand the applied load and to be failed in a tension-controlled manner [37,38]. Although, the replacement of tension steel only may lead to shifting the neutral axis of the RC section resulting in increased compression zone depth yielding compression-controlled failure that is unfavorable, refer to Fig. 1.

The adopted strengthening methodology in the current research work is based on providing strengthening materials on both tension and compression sides in order to balance the removed forces due to cut-out leading to an adequate global structural performance. Thus, the flexural capacity of the entire slab can be restored thoroughly. The tension side is strengthened by either NSM-steel bars or EB-CFRP sheets at both edges of the cut-out alongside the loading span, while the compression side is strengthened by either NSM-steel bars at both edges of the cut-out or an overlay of ECC material to be casted around the cut-out region.

2. Experimental work program

2.1. Test slabs

The experimental work program consisted of seven one-way slabs divided into three groups: one reference slab without cut-out and one control slab including cut-out referred to as the group No. 1, and five slabs including typical cut-out and strengthened using different techniques represented group No. 2 and group No. 3.

All slabs had the same concrete dimensions and internal steel reinforcement. Each slab had 600 mm width × 100 mm thickness and a total span of 1600 mm, while the center to center span was 1400 mm. The flexural reinforcement of the slabs consisted

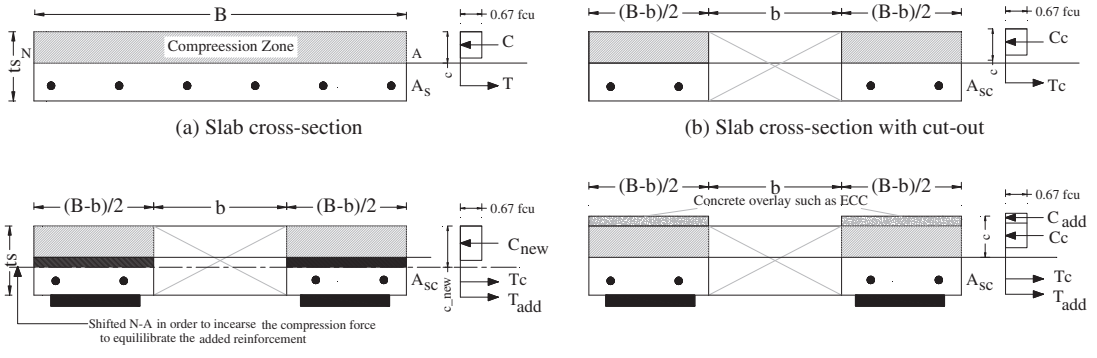


Fig. 1. Internal forces of slab cross-section including cut-out.

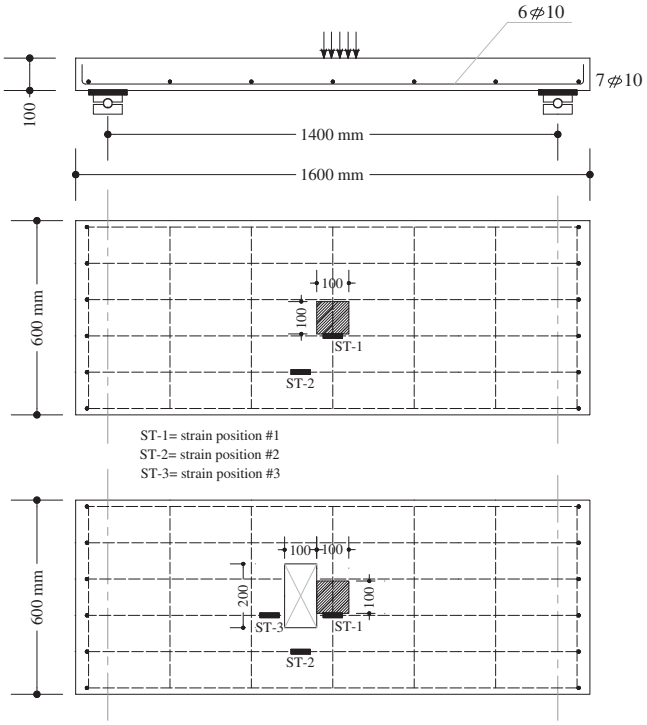


Fig. 2. Concrete dimensions and reinforcement detailing for un-strengthened slabs and base slabs for strengthened slabs.

of six high tensile steel bars of 10 mm diameter in the main direction and seven bars of 10 mm diameter as distributed steel in the transverse direction. The flexural reinforcement ratio was 0.92% and it is below the maximum reinforcement ratio allowed under the current ECP 203 and ACI 318-11 codes, in order to ensure tension failure of the slab. Fig. 2 shows the cross section and the reinforcement details for the un-strengthened slabs of group No. 1. Since the nominal strength of the structure does not depend on its size when geometrically similar structures are compared [39], the size effect analysis has been waived in the current research.

The strengthening technique for the tension side was based on either Near Surface Mounted steel bars (NSM-steel bars) or Externally Bonded Carbon Fiber Reinforced Polymer (EB-CFRP) sheets. Group No. 2 was based on the first technique (NSM-steel bars) included one slab strengthened in tension side by NSM-steel bar, one slab strengthened in both tension and compression sides by NSM-steel bars, and one slab strengthened in tension side by NSM-steel bars and in compression side by 20 mm thickness ECC overlay, simultaneously. The used steel bars for the NSM-steel bars were 10 mm diameter high tensile steel bars with 1000 mm length. Group No.3 included two slabs strengthened in tension side by EB-CFRP sheets and by 20 mm thickness ECC overlay at the compression side. The difference between the preceding slabs was that the ECC overlay of the second slab was reinforced by welded wire mesh of 100 mm × 100 mm with a wire diameter of 4 mm in order to reduce the volumetric changes. In addition, four shear connectors of 6 mm diameter were used in the form of shear dowels to hold the welded wire mesh to the reinforced concrete substrate. In addition, for the first slab, the surface of the RC substrate was prepared more properly than that of the second slab. Table 1 shows nomenclature and characteristics of all slabs.

Only the reference slab was casted without cut-out, while the remaining six slabs had a typical cut-out of 100 mm × 200 mm in cross-section located in middle part flash to the acting patch load as shown in Fig. 2.

All specimens were casted horizontally in wooden forms. Two days after casting, the standard cubes and the sides of the specimens were stripped from the molds and covered by plastic sheets. The upper surfaces of all specimens were cured by water until the seventh day, and then allowed air-drying until the testing day. After about one month, the concrete surfaces were prepared by abrasion, and then were thoroughly cleaned with compressed air before casting the ECC overlay for slabs SI-3, SII-1 and SII-2. Fig. 3 shows the strengthening configuration for group No. 2 and group No. 3.

2.2. Strengthening scheme

Here in, the adopted procedure for applying the strengthening materials for group No. 2 and group No. 3 are explained in details. For group No. 2, the method used in applying the NSM-steel bars was as follows: two 15 mm × 15 mm squarer grooves were cut in the desired direction into the concrete surface with one meter length, centered in the longitudinal direction, using a saw cutter machine. The grooves were filled halfway with epoxy paste, and then the steel bars were placed in the groove and lightly pressed. This forces the paste to flow around the bars and fill completely between them and the sides of the grooves. Finally, the grooves were filled with more paste and the surfaces were leveled. In order to eliminate the dust resultant from the sawing process, the grooves were cleaned with compressed air before bonding the steel bars to the concrete into to grooves. Before placing the steel bars into the

Table 1
Control slabs, nomenclature and characteristics of all slabs.

Group no.	Slab	Cube strength (MPa) for base RC slab	Cube strength (MPa) for ECC overlay	Characteristics	Objectives
1	S-C	33.45	–	Slab without cut-out	Control slab
	S-CO	33.45	–	Un-strengthened slab with cut-out	Effect of cut-out for un-strengthened slab
2	SI-1	29.22	–	Slab with cut-out strengthened in tension side only by NSM steel bars	Effect of tension strengthening only using NSM steel bars
	SI-2	29.22	–	Slab with cut-out strengthened in both tension and compression sides by NSM steel bars	Effect of both tension and compression strengthening using NSM steel bars
	SI-3	30.11	60.24	Slab with cut-out strengthened in tension side by NSM steel bars and in compression side by ECC overlay	Effect of ECC overlay in the compression side along with NSM steel bars in tension side
3	SII-1	31.03	61.35	Slab with cut-out strengthened in tension side by EB-CFRP sheets and in compression side by ECC overlay	Effect of ECC overlay in the compression side along with EB-CFRP sheets in tension side
	SII-2	31.03	61.35	Slab with cut-out strengthened in tension side by EB-CFRP sheets and in compression side by reinforced ECC with welded wire mesh	Effect of using welded wire mesh in the ECC overlay attached using shear connectors compared to proper surface preparation

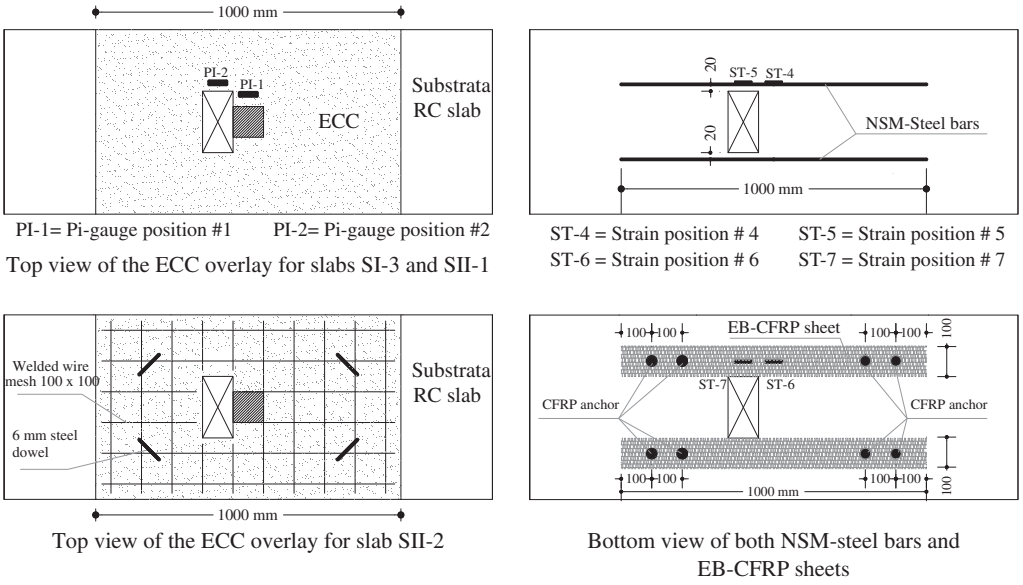


Fig. 3. Strengthening configuration for group No. 2 and group No. 3.

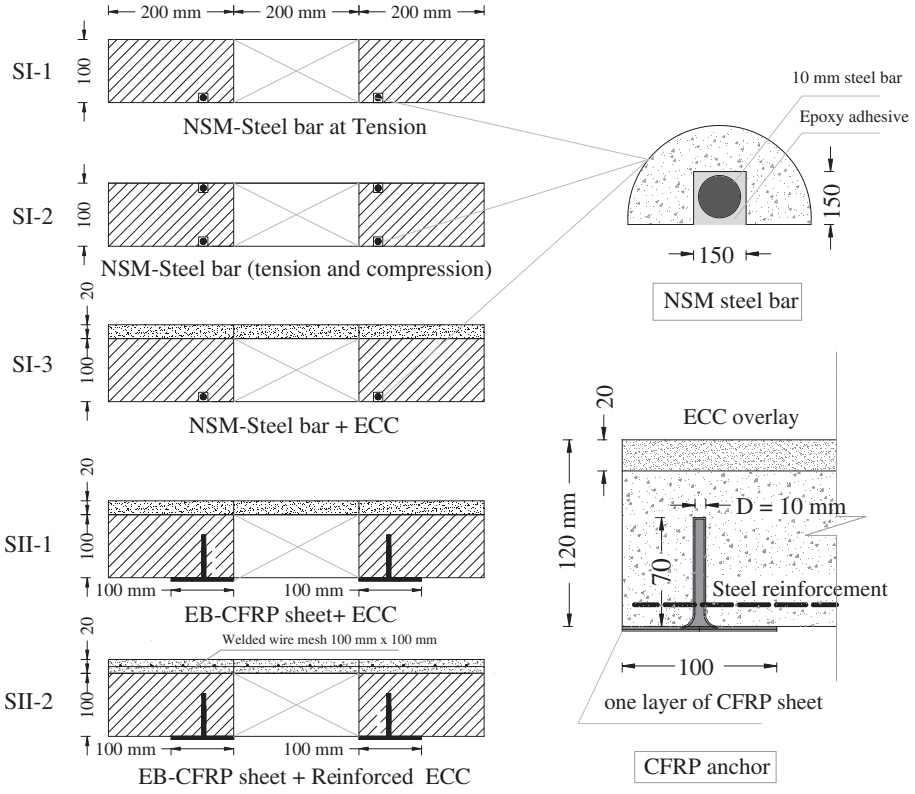


Fig. 4. Details of strengthening techniques for group No. 2 and group No. 3.

grooves, two strain gauges were mounted along steel bars in the mid-point and next to the cut-out location in order to record the developed strain during loading (ST-4 and ST-5 in Fig. 3).

As for group No. 3, both slabs were strengthened in tension side using carbon-fiber-reinforced polymers sheets, CFRP, in accordance with ACI-440 (2008) recommendations [5]. The strengthening schemes are demonstrated in Figs. 3 and 4. Since the adopted strengthened technique is considered as bond-critical application, surface preparation requirements should be based on the intended application of the CFRP system. The concrete surface was prepared with abrasive techniques. Two 100 mm width by 0.13 mm thickness CFRP sheets were used in the longitudinal directions next to the cut-out at both sides with 1000 mm length centered in the longitudinal direction. The CFRP sheets were anchored to the substrate RC slab by two anchors at each end using special CFRP anchors. The carbon fiber anchors were made by cutting a strip of the CFRP sheet, inserting it into a predrilled hole, and then fanning the ends of the anchor over the CFRP sheet as shown in Fig. 4.

The carbon fiber anchors were made from the same material as the sheet and were saturated with epoxy and inserted immediately before the sheet was placed. This process ensures that the anchors and sheet form a continuous composite unit. Inserting anchors into the core of the concrete slab at 70 mm ensures that stresses are transferred to the concrete and surrounding reinforcing steel, as well as ensuring that failure does not occur by separation of the concrete cover or de-bonding of the CFRP sheets [4,40–46]. All edges of the predrilled concrete holes were rounded to limit stress concentrations at the anchor bend. The total cross-sectional area of the anchors at both ends was taken two times the cross-sectional area of the longitudinal CFRP sheets. Two CFRP anchors were used for each side and located at 100 mm away from the free edge of the sheet.

For the 20 mm thickness ECC overlay used for slabs SI-3, SII-1 and SII-2, the contact surfaces of the RC substrates were roughened using chisel to remove slurry cement from external surfaces of coarse aggregates. The estimated roughness amplitude was about 8 mm for slabs SI-3 and SII-1, and about 3 mm for slab SII-2. Before placing the ECC layers, the contact surfaces of concrete substrates were re-cleaned with brush and high-pressure air to ensure a clean bonding surface, and then they were adequately damped [47].

2.3. Material properties

The used concrete was made from ordinary Portland cement (Type I), natural sand, and crushed pink limestone, as the coarse aggregate of maximum size of 12 mm, with a mixture proportions as reported in Table 2 in order to obtain concrete with target strength of 30 MPa. The actual compressive strength of the used concrete was determined at the testing day as the average of three standard cubes of 150 mm side length as reported in Table 1.

Engineered Cementitious Composites, ECC, was made with ingredients typically found in concrete, including ordinary Portland cement, sand, silica fume and superplasticizer based on poly-carboxylic ether. However, no coarse aggregate was employed. Instead, micro-fibers were added. The mix proportions of the ECC used as a strengthening material are listed in Table 2. Water to binder ratio (W/B) was 0.27. 10% of the design cement content was replaced by silica fume. High strength polypropylene fiber (PP) was selectively chosen and its volume in mix was 1%. The diameter and length of the PP fibers were 0.025 mm and 12 mm, respectively. The tensile strength of the used PP fibers was 626 MPa. PP Fiber can decline the brittleness of structure effectively by improving the continuity and uniformity of concrete and reduce the cracking obviously during plastic shrinkage.

The target compressive strength of the used ECC was designed to be 60 MPa, while the actual strength for each slab was determined based on the compressive test results of three standards cubes of 150 mm side as reported in Table 1.

In order to determine the mechanical properties of the used 10 mm diameter deformed high tensile steel bars, tensile tests were performed on three specimens. The mean value of tensile yield strength, ultimate strength and Young's modulus were 396 MPa, 631 MPa and 200 GPa, respectively. For the last slab, welded wire mesh was used in order to restrain the volumetric changes for the ECC overlay with bar diameter of 4 mm and spacing of 100 mm in both directions. The tensile yield strength and the ultimate strength of the bar were 413 MPa, 597 MPa, respectively. The welded wire mesh was held in position through four steel dowels of 6 mm diameter extruded from the base RC slab. These dowels had tensile yield strength and the ultimate strength as 274 MPa, 396 MPa, respectively. For NSM-steel bars, Sika 165 was used in order to resin the 10 mm steel bar into the pre-cut grooves.

Regarding the used CFRP sheets, carbon fiber fabric SikaWrap 230C/45 and epoxy based impregnating resin Sikadur-330 were implemented. Table 3 shows the mechanical properties for CFRP fabric sheet along with the epoxy resin as provided by the manufacturer.

Table 3
Mechanical properties of CFRP sheets.

Criteria	CFRP sheets	Epoxy
Tensile strength (MPa)	3500	30
Modulus of elasticity (GPa)	230	21.40
Failure strain (%)	1.50	4.80
Thickness (mm)	0.13	–

2.4. Test setup and instrumentation

One bay of three-dimensional steel frame as presented in Fig. 5 was equipped then used to carry out the testing. A 100 mm LVDT was used in order to measure the vertical deflection at mid-span point of the slab. While, 10 mm strain gauges were used in order to measure the developed strains in internal reinforcement at the tension side, NSM-steel bars and the CFRP sheets at positions shown in Figs. 2 and 3. In addition, a 100 mm gauge length Pi-gauge was used to measure the deformation at the concrete compression side. Hence, the concrete compressive strain can be obtained. The slab was loaded at the mid-point by patch load through a loading square steel plate of 100 mm side and 30 mm thickness. Therefore, in several steps the slab was loaded up to failure. The load on the slab was measured by a load cell of 600 kN capacity. A laser level was used to ensure the coincidence of the axes of the slab, load cell and the loading steel plate before testing.

After each loading step, the vertical mid-span deflection, the Pi-gauge readings, the strains in longitudinal steel in addition to the developed tensile strain in the NSM-steel bars and the CFRP sheets were recorded. The loading rate for all slabs ranged from 0.05 to 0.07 kN/s. An automatic data logger unit (TDS-102) had been used in order to record and store data during the test for load cell, steel strain gauges, CFRP strain gauges, Pi-gauges, and LVDT.

3. Results and discussion

The test results of the un-strengthened control slab and strengthened slabs are compared in order to verify the effectiveness of the adopted strengthening systems in restoring the load carrying capacity and stiffness reduced by the presence of the cut-out. Generally, all strengthened slabs achieved higher strength and stiffness than that of the corresponding control slab including cut-out without strengthening (S-CO). And some slabs achieved an

Table 2
Mix proportions of RC slabs and ECC overlay for one cubic meter (kg/m^3).

Concrete mix	W/B[a]	Cement	Sand	Coarse aggregate	Water	Silica fume	Super-plasticizer	PP fiber (12 mm)
RC	0.38	340	660	1320	130	–	–	–
ECC	0.27	1090	654	–	327	109	24	12

[a] W/B is the water/binder ratio, B = cement + silica fume.

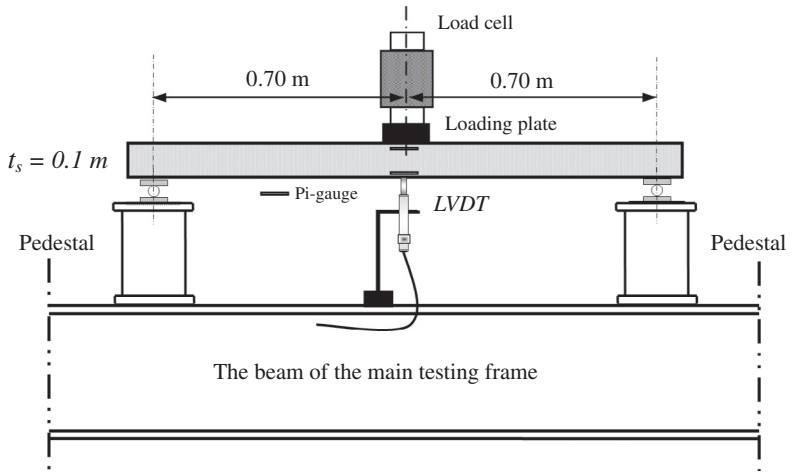


Fig. 5. Test setup.

Table 4
Failure characteristics of all slabs.

Group no.	Slab	P_{cr} (kN)	P_y (kN)	P_u (kN)	$\frac{P_u}{P_{u(S\text{-}CO)}}$	ε_u(steel), micro-strain	ε_u(NSM), micro-strain	ε_u(CFRP), micro-strain	Dominant mode of failure
1	S-C	18.8	43.7	56	1.49	5022	–	–	Flexural failure
	S-CO	12.9	34.1	37.7	1	4121	–	–	Flexural failure
2	SI-1	15.4	39.7	54.2	1.44	3871	4642	–	Flexural failure
	SI-2	17.1	45.3	48.3	1.28	2200	2471	–	Flexural failure followed by Punching shear at complete collapse
	SI-3	17.4	63.2	68.7	1.82	4193	6501	–	Flexural failure followed by one way shear at complete collapse
3	SII-1	21.5	60.4	63.4	1.68	3300	–	9411	Shear failure at cut-out location followed by rupture of CFRP sheets
	SII-2	24.7	53.3	56.1	1.49	4832	–	7123	Flexural failure at cut-out location followed by rupture of CFRP sheet

P_u = Total load at failure, P_{cr} = cracking load, P_y = yield load at main steel adjacent to cutout, ε_u(steel) = ultimate tensile strain at main steel adjacent to cutout, ε_u(-NSM) = ultimate tensile strain at the near surface mounted steel bars, ε_u(CFRP) = ultimate recorded tensile strain at CFRP sheet.

equal or even higher load carrying capacity than that of the reference slab without cut-out (S-C). A summary of the test results is given in Table 4 and further discussed as follows.

3.1. Failure behavior and crack patterns

First, it is very crucial to explain the load-transfer mechanism for the slab including cut-out in order to be able to expect the mode of failure for such slab. As shown in Fig. 6, the cut-out creates a break in the continuity of the slab loading trajectories in the middle of the slab. As a consequence, the patch load has to be transferred transversely in in-direct loading trajectories to the main slab strips next to the cut-out in both sides, then the load moves in direct loading trajectories to the supporting lines. The drawback associated with the presence of the cut-out is the weakness in the slab stiffness next to the acting patch load leading to the re-distribution of the acting load until it reaches the main supporting lines. Although the tested slab was one-way slab, transverse shear cracks at the cut-out face adjacent to the load could be formed due to the in-direct loading trajectories. It is worth mentioning that all tested slabs including cut-out either un-strengthened or strengthened developed such transverse shear cracks as will be shown later on the images of the failed slabs after the complete collapse.

The slab including cut-out could be failed in either flexural mode or shear mode as presented in Fig. 7. The flexural mode will be characterized by inclined cracks originated at the opening edges. On the other hand, shear mode of failure could be one-way shear if cracks developed as line AB or CD but most likely as CD line as presented in Fig. 7 or punching shear failure if the four cracking lines are connected at their ends.

Based on the experimental test results, five types of failure modes were observed. They are classified as normal flexural failure (Mode I), flexural-punching shear failure (Mode II), flexural–shear failure (Modes III), flexural-rupture of CFRP sheet failure (Mode IV) and flexural–shear-rupture of CFRP sheet failure (Mode V).

3.1.1. Mode I: Normal flexural failure

This failure is usually observed in under-reinforced slabs, and is characterized by the yielding of internal steel reinforcement in tension side, followed by crushing of concrete in compression. This failure occurred in the two un-strengthened slabs, slab S-C (without cut-out) and slab S-CO (including cut-out) in addition to one strengthened slab using NSM-steel bars in tension side only (SI-1).

For slab S-C without cut-out, failure occurred at mid-span section. Flexural cracks began to appear at the slab bottom face at a vertical load of about 32% of the ultimate load on the ascending branch. The flexural cracks increased uniformly in both propagation and width then widened significantly after the yield of steel reinforcement and concrete in compression crushed finally at the mid-span, as shown in Fig. 8(a and b).

For slab S-CO that contained cut-out, failure initiated at the section aligned with the cut-out edges. The flexural cracks widened

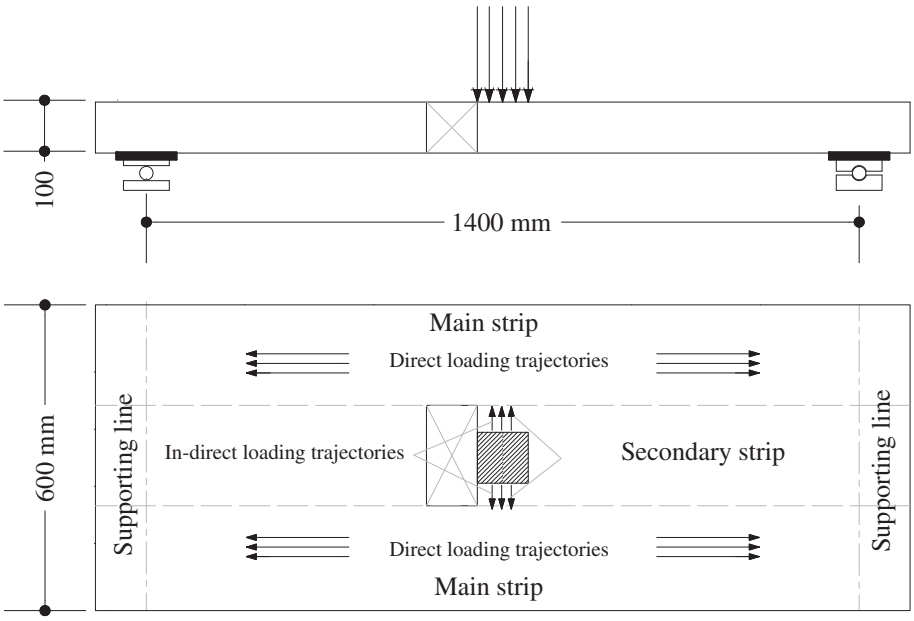
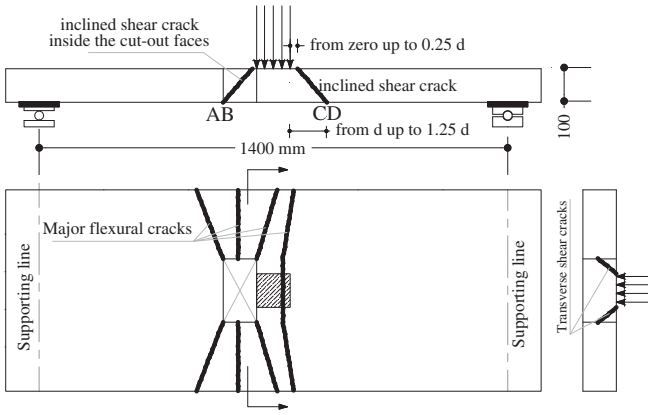
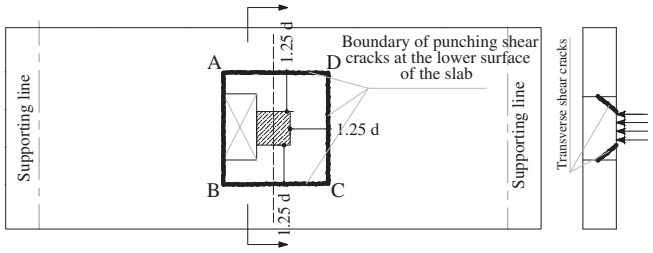


Fig. 6. Load transfer mechanism for slab including cut-out.



(a) Expected flexural failure at the bottom surface



(b) Expected shearl failure at the bottom surface

Fig. 7. Expected failure modes for slab including cut-out.

drastically after the yielding of steel reinforcement adjacent to the cut-out and concrete in compression crushed finally at the mid-span, as shown in Fig. 8(c and d). Before that, uniformly distributed flexural cracks were observed on the side face as well as the inside face of the opening in the span direction. In the region near the opening corners cracks were concentrated and propagated in an inclined direction to the longitudinal slab axis. On the transverse edge of the cut-out adjacent to the acting load, there were some diagonal cracks which originated from the bottom of the opening corner and propagated transversely in an inclined direction. This is because the large shear stress at the cut-out corners.

Slab SI-1 showed typical flexural failure as that observed for slab S-CO except that the numbers of developed cracks were higher and the corresponding widths were lower. That can be attributed to the effect of NSM mortar. The developed cracks were passed through the NSM mortar near the mid-span section, while these cracks were interrupted moving right and left to the mid-span section. In addition, at the complete failure state, the concrete cover was spalled out at the cut-out region for the main steel reinforcement while the mortar cover of the NSM-steel bars spalled out at the mid-span section as shown in Fig. 9(a).

3.1.2. Mode II: Flexural-punching shear failure

Although the tested slab was one-way slab, punching shear failure was developed in slab SI-2 as shown in Fig. 9(c and d). The failure began as flexural failure where cracks were developed in the tension side then increased with loading up to punching shear failure suddenly controlled the failure. That unexpected failure can be triggered by the transverse loading since the upper and lower NSM-steel bars presented pseudo-secondary beams, which attracted loading in transverse direction. As explained in Fig. 7, the longitudinal cracks due to the transverse shear loading connected with the transverse cracks due to the longitudinal shear loading resulted in the punching shear failure. It is worth mentioning that the slab SI-2 exhibited the lowest ultimate capacity among the slabs of the group No. 2 that used the NSM-steel bars as a strengthening technique, even compared with the slab SI-1 that use NSM-steel bar at tension side only. That means the approach of using NSM-steel bars at both tension and compression sides is unsuccessful and has to be avoided.

3.1.3. Mode III: Flexural–shear failure

Shear failure controls the failure when the flexural resistance exceeds the shear resistance. The slab SI-3 contained 20 mm thickness of ECC overlay. That ECC overlay was perfectly bonded to the RC slab due to properly surface preparation. Hence, the concrete cross-section was behaved as a composite section of 120 mm of to-



(a) Concrete crushing of concrete top surface of slab S-C



(b) Cracks propagation of the tension side of slab S-C



(c) Concrete crushing of concrete top surface of slab S-CO



(d) Failure around opening of slab S-CO

Fig. 8. Failure modes for all slabs of group No. 1.

tal thickness till a high level of loading. As expected in Fig. 7, the flexural cracks were developed and concentrated around the cut-out location till a load exceeding the ultimate load of the control slab (S-C), and then detachment between the ECC overlay and the RC substrate was noticed at the mid-span section. Hence, the flexural capacity was reduced allowed the development of shear cracks at the longitudinal inner faces of the cut-out till the complete failure occurred as shown in Fig. 9(d).

3.1.4. Mode IV: Flexural-shear-CFRP rupture

This failure was characterized by normal flexural failure that followed by shear failure in the inner longitudinal faces of the cut-out, then the CFRP rupture at the mid-span was ended the test. As expected in Fig. 7, flexural cracks were developed and concentrated around the cut-out location till a about 70% of the ultimate load on the ascending branch, and then shear cracks began to appear followed by de-bonding of the epoxy resin around the mid-span section. The de-bonding of the CFRP sheet occurred due to high local interfacial stress near wide cracks. The widening of the crack is the direct driving force of propagation, and the relative vertical displacement between the two faces of the crack produces the peeling stress on the interface. Regarding the cracks propagation, it was noted that the cracks were concentrated outside the region between the two CFRP sheets while most of these cracks were prevented from passing through the intermediate region between the CFRP sheets. The most important observation was that the end anchors behaved perfectly up to rupture of the CFRP sheets at their mid-span points which attributed to the sound installation of the end anchors. This type of failure occurred for slab SII-1 as presented in Fig. 10(a).

3.1.5. Mode IV: Flexural-CFRP rupture

Slab SII-2 exhibited this kind of failure mode. The de-bonding process initiated at a major flexural crack near the mid-span section and then propagated toward the end where the cut-out was located. When this occurred, the CFRP sheets were ruptured, as shown in Fig. 10(b), rather than de-bonding as a whole sheet. The de-bonding of the CFRP sheet occurred due to high local interfacial stress near wide cracks. The widening of the crack was the direct driving force of propagation, and the relative vertical displacement between the two faces of the crack produced the peeling stress on the interface. No failure of the end anchors was observed while the ruptures of both CFRP sheets were occurred near the mid-span of the slab. This behavior was developed as expected and presented in Fig. 7. The cracking behavior of slab SII-2 was similar to that of slab SII-1. However, no shear cracks were developed. That can be attributed to the lower flexural capacity of slab SII-2 which controlled the overall failure.

Comparing the behavior of the ECC overlay for specimens SII-1 and SII-2 shows that the surface preparation has a great effect than that the shear connector along with poor surface preparation effects. Fig. 11 shows that the ECC overlay still integrated to the RC substrate for slab SII-1 during all stages of loading even after complete failure of the slab. That can be attributed to the perfect surface preparation before installing the ECC overlay. On the other hand, fair surface preparation of slab SII-2 combined with 4 shear connectors between the ECC overlay and the RC slab could not guarantee the complete bond between them. Furthermore, detachment was observed near failure at lower acting load compared to that of slab SII-1.



(a) Bottom surface of slab SI-1 at complete collapse



(b) Punching of the top surface of slab SI-2



(c) Bottom surface of slab SI-2 at complete collapse

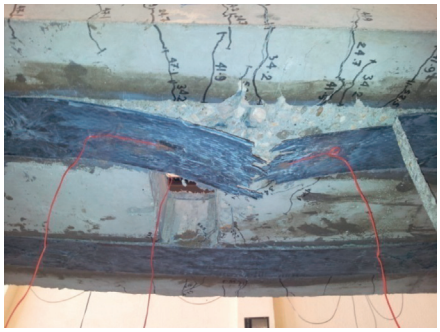


(d) Slab SI-3 at complete collapse state

Fig. 9. Failure modes for all slabs of group No. 2.



(a) Slab SII-1 after complete collapse



(b) Slab SII-2 after complete collapse

Fig. 10. Failure modes for all slabs of group No. 3.



(a) Slab SII-1



(b) Slab SII-2

Fig. 11. Effect of surface preparation on the bonding characteristics between ECC overlay and RC substrate.

3.2. Cracking and ultimate loads

Table 4 shows the results of the major flexural cracking load for all the un-strengthened and strengthened slabs once the cracking capacity of the concrete was exhausted. The un-strengthened slab including cut-out showed the lowest cracking load due to the effect of the cut-out in decreasing the cracking capacity of the slab. However, the percentages of the cracking load to the corresponding failure loads were approximately the same as that for the reference slab without cut-out, which was about 34%. For the group No. 2, the percentages of cracking loads to the corresponding ultimate loads ranged from 25% to 35%, inspite that the cracking loads for all specimens of that group were higher than that of the un-strengthened slab (S-CO). For group No. 3, the cracking loads showed higher loads compared to those of group No. 2. This can be attributed to the crack arresting action of the externally bonded CFRP sheets, which altered the cracking propagation compared to that of the NSM-steel bars technique. The highest percentage of the cracking load to the relevant ultimate load was recorded for slab SII-2, which was about 44%.

Based on the recorded values of the ultimate load carrying capacities for all slabs in Table 4, it can be concluded that all strengthened slabs achieved higher capacity than that of un-strengthened slab included cut-out (S-CO). These increases were 44%, 28%, 82%, 68%, and 49%, respectively, for slabs SI-1, SI-2, SI-3, SII-1 and SII-2. However, slabs SI-3, SII-1, and SII-2 could only restore the full capacity of slab without cut-out (S-C) and showed increases of about 23%, 13% and 0.2%, respectively, above the corresponding strength of the reference slab S-C. That can be attributed to the effect of the 20 mm ECC overlay, which increased the total depth of the slab by 20% that led to increased lever arm of the moment resisting of the concrete section.

From the strength viewpoint, slab SI-3 showed the highest ultimate capacity which incorporated the NSM-steel bars in tension side and the ECC overlay in the compression side. That highlighted the superiority of the NSM-steel bars technique over the EB-CFRP technique.

3.3. Load–deflection relationships

The load–deflection relationships are shown in Figs. 12 and 13 for all slabs. Each slab exhibited linear behavior up to the cracking load. Beyond that, a rapid change in the slope of the load–deflection curve was observed. With further loading, the yielding of the internal steel reinforcement occurred in un-strengthened slabs S-C and S-CO, and then a plateau in the load deflection curve was observed soon after that till the complete failure of the un-strengthened slabs. As for strengthened slabs, the manifested load–deflection plateaus after yielding were varied according to the relevant strengthening techniques.

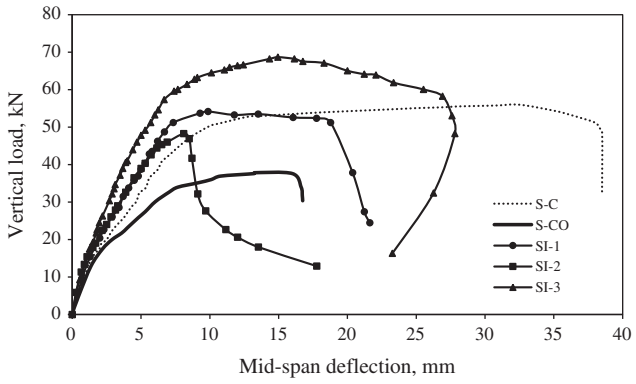


Fig. 12. Comparison among load–deflection relationships for all slabs of group No. 2 in addition to control group.

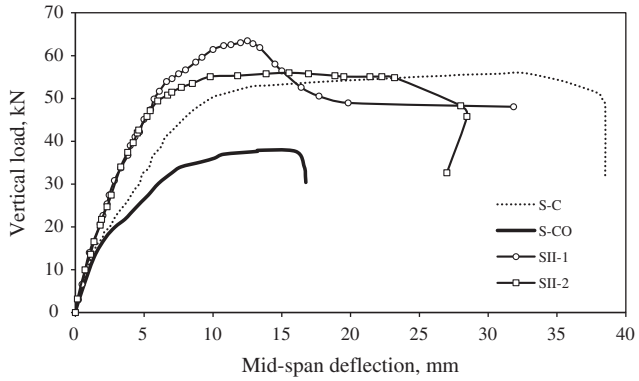


Fig. 13. Comparison among load–deflection relationships for all slabs of group No. 3 in addition to control group.

To highlight the effectiveness of the NSM-steel bars technique in restoring the load carrying capacity of slabs included cut-out, the load–deflection curves are compared as shown in Fig. 12. For the three strengthened slab, both strength and stiffness were enhanced significantly. Both strengthened slabs SI-1 and SI-2 showed approximately identical behavior till the yielding of internal reinforcement, and then a sudden drop in the ultimate capacity of slab SI-2 was noticed due to the un-expected punching failure. However, the slab SI-1, which uses NSM-steel bars in tension side only, exhibited improved behavior compared to that of slab SI-2. The slab SI-3 showed distinguished behavior among all slabs of the group No. 2 from the viewpoints of strength, stiffness.

To highlight the effectiveness of the EB-CFRP technique in restoring the load carrying capacity of slabs included cut-out, the load–deflection curves are compared as shown in Fig. 13. For both strengthened slabs, both strength and stiffness were enhanced significantly compared to those of un-strengthened slabs. In addition, the full capacity of the slab without cut-out was restored and outperformed for both slabs. Both slabs (SII-1 and SII-2) showed approximately identical behavior till the commencement of detachment of the ECC overlay of slab SII-2 due to improper surface preparation, and then a steady plateau was notice until the substrate RC slab was failed accompanying with the CFRP rupture at the mid-span of the slab. On the other hand, slab, SI-1 showed higher capacity than that of slab SII-2 due to the composite action between the RC substrate and the ECC overlay that was maintained up to failure due to complete bond provided by the proper surface preparation. A sudden drop in the ultimate capacity of slab SI-1 was noticed after attaining the ultimate capacity that was attributed to the sudden rupture of the CFRP sheets.

Another comparison criterion for all slabs is the initial stiffness. The initial stiffness is the slope of the first part of the load–deflection curve. Figs. 12 and 13 represent comparison among all slabs for group No. 2 and group No. 3, respectively. The normalized initial stiffness for the reference slab without cut-out, slab S-C, with respect to that of un-strengthened slab with cut-out, S-CO is 1.15. That means the introduced cut-out reduced the initial stiffness of the slab by about 15%.

As for group No. 2, with the aid of Fig. 12, the calculated normalized initial stiffness for slabs SI-1, SI-2 and SI-3 are 1.28, 1.55, and 1.61, respectively, with respect to that of slab S-CO. That means the adopted strengthening scheme for that group assessed in restoring the initial stiffness by about 28%, 55% and 61%, respectively, for slabs SI-1, SI-2 and SI-3, which are higher than the initial stiffness lost due to introducing the cut-out. With the aid of Fig. 13, it can be

concluded that the initial stiffness of the slabs SII-1 and SII-2 are restored by approximately the same percentage which is 85%.

The above comparison represented the elastic range of loading. However, this behavior can be tolerated to the in-elastic range where the load–deflection curves presented that the developed central deflections for all slabs of group No. 2 and group No. 3 are lower than those of reference slab S-C and control slab S-CO at the same loading level, leading to increased instantaneous stiffness.

As an approximation, the secant stiffness at the yielding condition can be calculated as the yielding load divided by the corresponding deflection and can be compared for all slabs. The normalized secant stiffnesses are 1.52, 1.44, 2.87, 2.44, and 2.39 for slabs SI-1, SI-2, SI-3, SII-1, and SII-2, respectively, with respect to that of slab S-CO. It can be seen that slab SI-3 exhibited the highest stiffness restoration among all slabs. It is worth mentioning that the same slab, SI-3, exhibited the highest ultimate capacity that assure the dominance of the adopted strengthening technique which accompanied the NSM-steel bars along with the ECC overlay.

3.4. Steel strain

Fig. 14 shows the relationships between the vertical loads and the corresponding tensile strains at the continuous steel bars adjacent to the cut-out. It can be seen that all tensile strains exceeded the yielding point. Although, the slab SI-2 failed suddenly due to punching shear failure, its tensile strain reached the yield point before such failure. The slab SI-3 showed the superior behavior since it exhibited the lowest developed tensile strain at the same loading level among all strengthened slabs.

The recorded tensile strain at the mid-span points of the NSM steel bars for all slabs of group No. 2 showed the same trend as that of the internal steel bars as presented in Fig. 15. However, the developed strains were higher than that the relevant developed stains in the internal steel bars, which can be attributed to the increased distance from the neutral axis of the concrete cross-section.

3.5. CFRP strain

For group No. 3, the group adopted EB-CFRP sheets along with ECC overlay, the tensile strains were measured at the mid-point and next to the cut-out of the CFRP sheets at positions ST-6 and ST-7 as illustrated in Fig. 3. As reported in Table 4, it can be noted that the measured strains were 63% and 47% of the failure strain of the CFRP sheets for slab SII-1 and SII-2, respectively. However, the

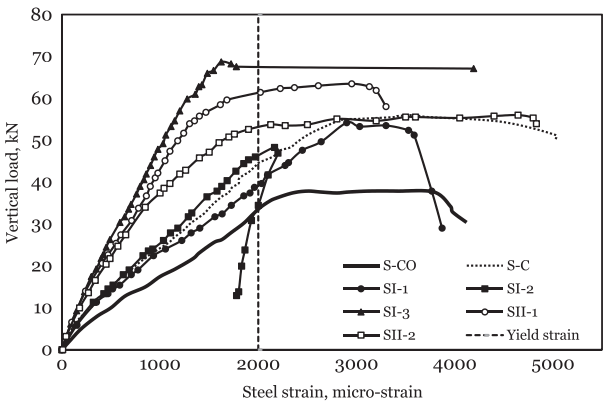


Fig. 14. Vertical load versus developed steel strain in the continuous steel bar adjacent to cut-out for all groups (Strain ST-2 in Fig. 2).

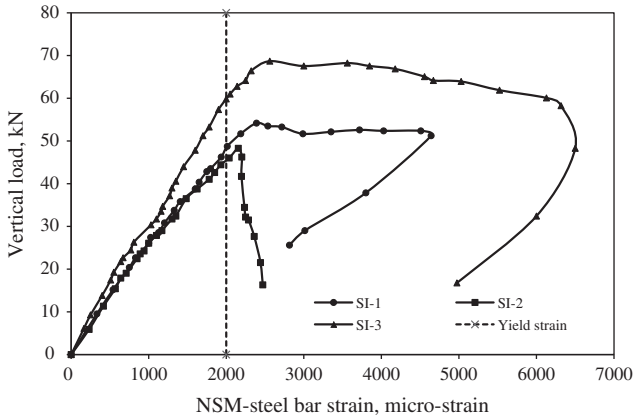


Fig. 15. Vertical load versus developed steel strain in the NSM steel bar adjacent to cut-out for all slabs of group No. 2 (strain ST-4 in Fig. 3).

CFRP sheets were reached the rupture strain near failure since the CFRP sheets were ruptured around the mid-span points. That can be attributed to the properly detailed anchors at both ends of the CFRP sheets that did not allow the de-bonding failure at the ends and enabled the CFRP sheets to utilize their full tensile capacity.

3.6. Ductility

Ductility may be broadly defined as the ability of a structure to undergo inelastic deformations beyond the initial yield deformation with no decrease in the load resistance. Ductility has generally been measured by a ratio called the ductility index or factor (μ). The ductility index is usually expressed as a ratio of rotation (θ), curvature (φ), deflection (displacement) (Δ), and absorbed energy (E) at failure divided by the corresponding property when the steel starts yielding. In the current study, ductility has been estimated based on both displacement and absorbed energy methods.

3.6.1. Displacement-based ductility

Fig. 16 shows schematically the typical load–deflection response of the RC slab. Point A corresponds to the first steel yielding at the main tension steel adjacent to the cut-out, and point B to failure. Based on Fig. 16, the displacement ductility index is defined by Eq. (1) [48]:

$$\mu_{\Delta} = \frac{\Delta_u}{\Delta_y} \tag{1}$$

where (Δ_u) is the mid-span deflection at ultimate slab load and (Δ_y) is the mid-span deflection at yielding load of the tensile steel reinforcement adjacent to the cut-out.

Table 5 shows the experimental values of (Δ_u), (Δ_y), the displacement ductility index value of (μ_{Δ}) for all slabs. It can be seen that the un-strengthened slab including cut-out (S-CO) developed the highest yielding deflection compared to all strengthened slabs and the lowest deflection at failure. As a consequence, the lowest displacement ductility was obtained for slab S-CO. The percentages of increases in displacement ductility indexes are 70%, 12%, 104%, 158% and 146%, respectively, for slabs SI-1, SI-2, SI-3, SII-1 and SII-2 compared to that of slab S-CO. The slab SII-1 showed the highest ductility index. However, it cannot restore the full ductility of slab without cut-out (S-C). It attained only 86% of the corresponding ductility of the reference slab S-C. On the other hand, the slab SI-3, which achieved the highest capacity cannot achieve the highest ductility. That means it a matter of compromise to decide which criteria is the most important for the assigned system, strength or ductility. The most significant observation was that

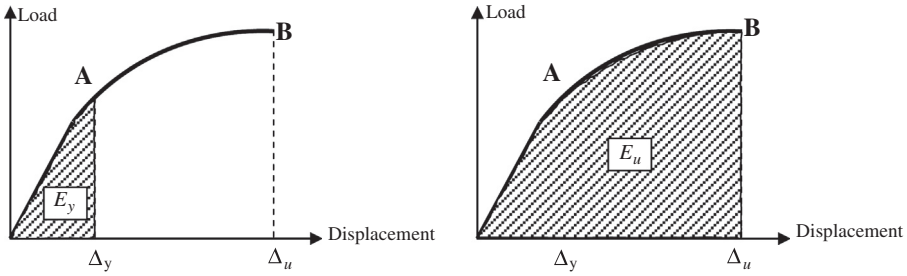


Fig. 16. Definition of key parameters for displacement and energy ductility.

Table 5
Ductility indices for test slabs.

Group no.	Slab	Δ_y (mm)	Δ_u (mm)	$\mu_\Delta = \frac{\Delta_u}{\Delta_y}$	$\frac{\mu_\Delta}{\mu_{\Delta(S\text{-}CO)}}$	E_y (kN m)	E_u (kN m)	$\mu_E = \frac{E_u}{E_y}$	$\frac{\mu_E}{\mu_{E(S\text{-}CO)}}$
1	S-C	5.3	38.5	7.2	3	107	1855	17.3	4.9
	S-CO	7.03	16.7	2.4	1	144	497	3.5	1
2	SI-1	5.3	21.6	4.1	1.7	137	935	6.8	1.9
	SI-2	6.5	17.8	2.7	1.1	181	467	2.6	0.7
	SI-3	4.7	23.3	4.9	2.1	145	1577	10.9	3.1
3	SII-1	5.1	31.8	6.2	2.6	129	1544	12	3.4
	SII-2	4.6	27.0	5.9	2.5	111	1387	12.5	3.6

Δ_y = Mid-span deflection at yielding, Δ_u = mid-span deflection at failure state, μ_Δ = deflection ductility index.
E_y = Energy of the system at yielding load, E_u = energy of the system at failure state; μ_E = energy ductility index.

slab SI-2 exhibited the lowest capacity and ductility among all strengthened slab. This assures that the strengthening technique using upper and lower NSM-steel bars in order to compensate the reduced capacity is unfavorable.

3.6.2. Energy-based ductility

Another method of determining ductility is based on the energy definition which is illustrated in Fig. 16. The energy ductility index (μ_E) as presented in Eq. (2) [49] is defined as the ratio between the energy of the slab at failure (E_u) and the energy of the slab at yielding load of tensile steel reinforcement adjacent to the cut-out (E_y).

$$\mu_E = \frac{E_u}{E_y} \tag{2}$$

The failure energy at the slab ultimate load (E_u), elastic energy at the first steel yield load (E_y), and the energy ductility index (μ_E) for all slabs are given in Table 5. Dissimilar to the displacement ductility index, the lowest energy ductility was obtained for slab S-CO compared to all strengthened slabs except slab SI-2, which showed lower ductility by about 25% to that of un-strengthened slab (S-CO). The percentages of increases in energy ductility indexes are 94%, 211%, 243% and 257%, respectively, for slabs SI-1, SI-3, SII-1 and SII-2 compared to that of slab S-CO. It can be seen that in both schemes, the EB-CFRP sheet strengthening technique showed higher ductility indices compared to those of the NSM-steel bars technique while it showed lower ultimate load carrying capacities. This observation is matching with the results obtained by Smith et al. [50] that the CFRP anchors was effective in delaying the de-bonding and also was effective in enhancing the deformability and ductility of RC slabs strengthened in flexure with FRP plates.

3.7. Experimental capacity versus design capacity

For all slabs, the minimum design capacity are obtained analytically based on sectional analysis of the slab cross-section considering the critical section of width 400 mm for the slab included cut-out. The equivalent stress block analysis was implemented in order to carry out this task considering the following assumptions:

- The maximum steel stress is the yield stress for both internal longitudinal reinforcement and the NSM-steel bars inspite that the actual stresses exceeded the yielding stresses.
- The actual concrete characteristic strength for both RC slab and the ECC overlay is taken for each slab as reported in Table 1.
- The actual CFRP recorded strains as given in Table 4 are implemented in the analysis, which when multiplied by the modulus of elasticity as presented in Table 3 give the CFRP actual stresses.
- Complete bond between the EB-CFRP sheets and the RC substrate is assumed.
- Complete bond between the RC substrate and the ECC overlay is assumed. In addition, the effect of the internal wire mesh in the ECC layer of slab S-II-2 is neglected.

Table 6
Experimental ultimate loads versus design ultimate loads for all slabs.

Group no.	Slab	$P_{experimental}$ (kN)	P_{design} (kN)	$P_{experimental}/P_{design}$
1	S-C	56.0	41.99	1.33
	S-CO	37.7	27.99	1.35
2	SI-1	54.2	40.13	1.35
	SI-2	48.3	39.59	1.22
	SI-3	68.7	54.28	1.27
3	SII-1	63.4	54.1	1.17
	SII-2	56.1	49.83	1.13

Table 6 shows the obtained design capacities for all slabs. Comparison between the experimental capacities and the minimum design capacities revealed that the actual capacity of the slab including cut-out can be obtained analytically with a safety margin of about 35% for un-strengthened slabs. As for the strengthened slab using NSM-steel bars, the safety margin can be reduced to be 22% due the complicated actual behavior while that margin is

reduced to 13% for the EB-CFRP technique. The safety margin of the EB-CFRP is based mainly on the efficiency factor of the CFRP that can reach to 0.5 as specified by FIB [12].

4. Conclusions

Based on the studied strengthening techniques of reinforced concrete one-way slabs including cut-out around the mid-span, loading scheme, and according to the used concrete dimensions and reinforcement detailing, the following conclusions maybe drawn:

1. Properly designed and detailed end anchors for EB-CFRP sheets prevented the de-bonding of both ends of the sheets till the CFRP sheets ruptured around the mid-span of the slab. They enabled the CFRP sheets to utilize their full tensile capacity resulted in the full restoration of the flexural capacity of both slabs strengthened with CFRP sheets in the tension side (slabs SII-1 and SII-2). After the CFRP sheet ruptured, de-bonding of both CFRP sheets for both slabs were observed and extended to the end anchors locations.
2. Surface preparation of the substrate RC slab before casting the ECC overlay showed great influence on the composite action between the ECC overlay and the RC substrate. The rightfully prepared slab showed full bond till the complete failure occurred without any detachment of the ECC overlay. Comparing the two slabs SII-1 and SII2 showed that the sound surface preparation of slab (SII-1) enabled it to restore the full flexural capacity of the un-cut slab and outperform its structural performance compared to that of slab with poor surface preparation (SII-2) insipte that the ECC overlay of later slab (SII-2) had welded wire mesh attached to the RC substrate by four steel dowels.
3. Among all strengthened slabs, slab SI-3 that adopted NSM-steel bars along with ECC overlay technique showed the highest flexural capacity. It restored the ultimate flexural capacity of unstrengthened slab including cut-out and outperform its capacity than that of the reference slab without cut-out by about 23%.
4. It a matter of compromise to decide which criteria is the most important for the assigned system, strength or ductility taking into account the cost of the strengthening technique since the slab SI-3 exhibited the highest ultimate capacity, while slab SII-1 or SII-2 exhibited the highest ductility based on the adopted scheme (displacement-based or energy-based).
5. Using thin layer of ECC material of 20% the slab total thickness in the compression side ensured the full restoration of the flexural capacity due to cut-out when combined with either NSM-steel bars or EB-CFRP sheets in the tension side.

References

[1] Smith ST, Kim SJ. Strengthening of one-way spanning RC slabs with cutouts using FRP composites. Constr Build Mater 2009;23:1578–90.
[2] Boon KH, Diah AM, Loon LY. Flexural behavior of reinforced concrete slab with opening. In: Proceedings of MUCEET2009, Malaysian technical universities conference on engineering and technology, June 20–22, 2009, MS Garden, Kuantan, Pahang, Malaysia.
[3] Florut S, Stoian V, Diaconu D. Issues and provisions for design and strengthening of RC slabs with cut-outs. In: Conference on civil engineering infrastructure based on polymer composites, CECOM, 2012, November 22–23, Krakow, Poland.
[4] Kim SJ, Smith ST. Strengthening of RC slabs with large penetrations using anchored FRP composites. In: The second official international conference of international institute for FRP in construction for Asia–Pacific region. Seoul, Korea, 2009, 9–11 December 2009.
[5] ACI 440.2R-08. Guide for the design and construction of externally bonded FRP system for strengthening concrete structures. ACI committee 440. Farmington Hills (MI): American Concrete Institute; 2008. 45 pp.
[6] Ombres L. Prediction of intermediate crack de-bonding failure in FRP-strengthened reinforced concrete beams. Compos Struct 2010;92:322–9.
[7] Rasheed HA, Harrison RR, Peterman RJ, Alkhrdaji T. Ductile strengthening using externally bonded and near surface mounted composite systems. Compos Struct 2010;92:2379–90.
[8] Jumaat MZ, Rahman MM, Rahman MA. Review on bonding techniques of CFRP in strengthening concrete structures. Int J Phys Sci 2011;6:3567–75.
[9] Cromwell JR, Harries KA, Shahrooz BM. Environmental durability of externally bonded FRP materials intended for repair of concrete structures. Constr Build Mater 2011;25:2528–39.
[10] Benzarti K, Freddi F, Frémond M. A damage model to predict the durability of bonded assemblies. Part I: De-bonding behavior of FRP strengthened concrete structures. Constr Build Mater 2011;25:547–55.
[11] Blaschko M, Zilch K. Rehabilitation of concrete structures with CFRP strips glued into slits. In: Proceeding of the 12th international conference on composites materials. Paris; 5–9 July 1999.
[12] FIB. Externally bonded FRP reinforcement for RC structures – technical report on the design and use of externally bonded fiber reinforced polymer reinforcement (EBR-FRP) for reinforced concrete structures; 2001. 138p.
[13] Tarek H, Rizkalla S. Investigation of bond in concrete structures strengthened with near surface mounted carbon fiber reinforced polymer strips. J Compos Constr 2003;7:248–57.
[14] Barros JA, Fortes AS. Flexural strengthening of concrete beams with CFRP laminates bonded into slits. Cem Concr Compos 2005;27:471–80.
[15] Kotynia R. Strengthening of reinforced concrete structures with near surface mounted FRP reinforcement. In: The 5th international conference, AMCM, Gliwice, Ustron, 12–14 June 2005.
[16] Asplund SO. Strengthening bridge slabs with grouted reinforcement. J ACI 1949;20:397–406.
[17] Walser R, Steiner W. Strengthening a bridge with advanced materials. Struct Eng Int (IABSE) 1997;2:110–2.
[18] Barros JA, Sena-Cruz JM. Strengthening a pre-stressed concrete slab by epoxy-bonded FRP composites and SFRC overlayer. In: Proceedings of the 7th international conference on inspection, appraisal, repairs and maintenance of buildings and structures. Nottingham Trent University, United Kingdom; 2001. p. 211–8.
[19] Bonaldo E, Castro-Gomes JP, Barros JA, Lourenço PB. SEM analysis of bond epoxy based layer between hardened concrete and SFRC repairing. In: Proceedings of the 10th Euro-seminar on microscopy applied to building materials – EMABM. University of Paisley, Scotland; 2005a. p. 15.
[20] Bonaldo E, Barros JA, Lourenço PB. Bond characterization between concrete substrate and repairing SFRC using pull-off testing. Int J Adhes 2005;25:463–74.
[21] Bolander JE, Berton S. Simulation of shrinkage induced cracking in cement composite overlays. Cem Concr Res 2004;26:861–71.
[22] Barros JA, Cunha VM, Ribeiro AF, Antunes JA. Post-cracking behavior of steel fiber reinforced concrete. Mater Struct 2005;38:47–56.
[23] Li VC. From micromechanics to structural engineering: the design of cementitious composites for civil engineering applications. JSCE, J Struct Mech Earthq Eng 1993;10:37–48.
[24] Li M, Li VC. High-early-strength ECC for rapid durable repair: material properties. ACI Mater J 2011;108:3–12.
[25] Li VC, Tailoring ECC. For special attributes: a review. Int J Concr Struct Mater 2012;6:135–44.
[26] Dhawale AW, Joshi VP. Engineered cementitious composites for structural applications. Int J Appl Innovat Eng Manage (IJAIEM) 2013;2:198–205.
[27] Li VC, Li M. Durability performance of ductile concrete structures. In: Proceedings of the 8th international conference on creep, shrinkage and durability of concrete and concrete structures. Ise-Shima, Japan; 2008. p. 761–8.
[28] Sahmaran M, Li M, Li VC. Transport properties of engineered cementitious composites under chloride exposure. ACI Mater J 2007;104:604–11.
[29] Li M, Li VC. Cracking and healing of engineered cementitious composites under chloride environment. ACI Mater J 2011;108:333–40.
[30] Fischer G, Li VC. Effect of fiber reinforcement on the response of structural members. Eng Fract Mech 2007;74:25–272.
[31] Li VC. Reflections on the research and development of engineered cementitious composites (ECC). In: Proceedings of the JCI international workshop on ductile fiber reinforced cementitious composites (DFRCC) – application and evaluation, DFRCC-2002, Takayama, Japan, October 21–22. p. 1–21.
[32] Alkhrdaji T, Nanni A, Chen G, Barker M. Upgrading the transportation infrastructure: solid RC decks strengthened with FRP. Concr Int: Des Constr 1999;21:37–41.
[33] Vasquez A, Karbhari VM. Fiber-reinforced polymer composite strengthening of concrete slabs with cutouts. ACI Struct J 2003;100:665–73.
[34] Casadei P, Ibell TJ, Nanni A. Experimental results of one-way slabs with openings strengthened with CFRP laminates. In: Proceedings, fibre-reinforced polymer reinforcement for concrete structures, FRPRCS – 6, 8–10 July, Singapore; 2003. p. 1097–106.
[35] Tan KH, Zhao HD. Strengthening of openings in one-way reinforced concrete slabs using carbon fiber-reinforced polymer systems. J Compos Constr, ASCE 2004;8:393–402.
[36] Seliem HM, Sumner EA, Seracino R, Smith ST. Field testing of RC slabs with openings strengthened with CFRP. In: Fourth international conference on FRP composites in civil engineering (CICE2008), 22–24 July 2008, Zurich, Switzerland.

[37] American Concrete Institute, ACI. Building code requirements for structural concrete (ACI 318-11) and commentary. Farmington Hills: ACI; 2011.
[38] Egyptian code for design and construction of reinforced concrete structures (ECP 203-2007); 2007.
[39] Bazant ZP. Size effect. Int J Solids Struct 2000;37:69–80.
[40] Orton SL, Jirsa JO, Bayrak O. Design considerations of carbon fiber anchors. J Compos Constr 2008;12:608–16.
[41] Zhang HW, Smith ST. FRP-to-concrete joint assemblages anchored with multiple FRP anchors. Compos Struct 2012;94:403–14.
[42] Breñ SF, McGuirk GN. Advances on the behavior characterization of FRP-anchored Carbon Fiber-Reinforced Polymer (CFRP) sheets used to strengthen concrete elements. Int J Concr Struct Mater 2013;7:3–16.
[43] Bank L. Progressive failure and ductility of FRP composites for construction: review. J Compos Constr 2013;17:406–19.
[44] Kalfat R, Al-Mahaidi R, Smith S. Anchorage devices used to improve the performance of reinforced concrete beams retrofitted with FRP composites: state of the art review. J Compos Constr 2013;17:14–33.
[45] Biolzi L, Ghittoni C, Fedele R, Rosati G. Experimental and theoretical issues in FRP–concrete bonding. Constr Build Mater 2013;41(4):182–90.
[46] Vanin A, Foraboschi P. New methods for bonding FRP strips onto masonry structures: experimental results and analytical evaluations. Compos: Mech, Comput, Appl, Int J 2013;4(1):1–23.
[47] Li VC. High performance fiber reinforced cementitious composites as durable material for concrete structure repair. Int J Restor Build Monum 2004;10:163–80.
[48] Bonaldo E, Oliveira de Barros JA, Lourenço PB. Efficient strengthening technique to increase the flexural resistance of existing RC slabs. J Compos Constr 2008;12:149–59.
[49] Thomsen HH, Spacone E, Limkatanyu S, Camata G. Failure mode analysis of reinforced concrete beams strengthened in flexure with externally bonded fiber-reinforced polymers. J Compos Constr 2004;8:123–31.
[50] Smith ST, Hu S, Kim SJ, Seracino R. FRP-strengthened RC slabs anchored with FRP anchors. Eng Struct 2011;33(4):1075–87.